

# TESTING TRANSPARENT BOUNDARY CONDITIONS FOR THE SHALLOW WATER EQUATIONS IN A NESTED ENVIRONMENT.

A McDonald  
Met Éireann  
Dublin, Ireland.

## 1. INTRODUCTION

In 1996 the HIRLAM group decided to re-examine the treatment of the artificial lateral boundaries of their limited area model with a view to improving it. Based on a review of the meteorological literature McDonald (1997) outlined the options used in various meteorological models and made non-radical recommendations on possible improvements to the HIRLAM lateral boundary treatment. By non-radical I mean only a modest commitment of resources would be required, and the boundary treatment would continue to be one of those used traditionally in operational meteorological models. These traditional methods are typically over twenty years old, and in the meantime new ideas on how to treat artificial boundaries have been pursued in other disciplines.

Increasing computer power has resulted in many limited area forecast models being run in a nested environment. In such a set-up the inner area can be small enough that any outgoing waves reflecting from the boundaries can quickly spread to the central area of interest, corrupting the forecast. Also, such an area can be small enough that a rapidly moving and rapidly deepening depression will cross it during the forecast period. (This is possibly the most important forecasting situation we deal with, because of its potential for devastation and loss of life). For much of the time the forecast will be dominated by the information which has previously entered via the inflow boundaries. For these reasons it is essential that our treatment of the boundary conditions be as close to perfect as we can make it.

The most popular method of treating the boundaries in operational models is to define a ‘relaxation zone’ next to the boundary within which all of the fields are relaxed toward the externally supplied ‘host’ model coarse mesh fields; see Davies (1976). On the boundary line itself the host model fields are imposed. Within the relaxation zone these fields are combined with the fields of the fine-mesh inner area (the ‘guest’ area) in such a way that the noise generated by the over-specification on the boundary is damped, while simultaneously the meteorological information is allowed to enter the area with minimum distortion. This is to some extent a balancing act, which is achieved by a careful choice

of (a) the relaxation parameters and (b) the width of the relaxation zone; see Källberg (1977).

Since the purpose of this report is to examine alternatives to the flow relaxation scheme let us list its perceived strengths and weaknesses.

*Strengths.* (a) Stable. (b) Robust. (c) Easy to implement. (d) Computationally inexpensive.

*Weaknesses.* (e) There is evidence that it can cause mass loss or gain; see McDonald (1998). (f) At points at which the characteristics are pointing out of the domain of integration we are imposing the host model solution when we do not need to. Thus we may introduce unnecessary errors when these fields are incorrect (as they will be in an operational environment). (g) The host and guest model fields will both normally be in approximate geostrophic balance. The scheme destroys this balance throughout the the boundary relaxation zone when the host and guest model velocities differ; see Cats and Åkesson (1983). (h) There are undefined parameters. The width of the boundary relaxation zone is undetermined. Let us assume its width is  $(N + 1)\Delta x$ . Then there are  $N$  undefined parameters which must be determined either ‘experimentally’, as in Källberg (1977) or by using plausibility arguments as in Davies (1983) or Lehmann (1993). It is probable that these parameters will have to be re-tuned for finer grids. (i) It has not been built from solid mathematical foundations: we are no longer solving the equations of motion, but a new set of equations with very different mathematical properties. In the past, when the boundaries were far removed from the area of interest, pragmatists were not particularly bothered by this point. However, as we argued above, in a nested environment there may be situations when the boundaries will have more influence on the forecast than the initial conditions. Consider the mathematical effort that has been expended on creating the best possible initial fields: optimal interpolation, 3DVAR, 4DVAR. If we are to make equally efficient use of the boundary data it will be necessary to put more effort into making our boundary treatment mathematically sound.

From the very beginning it was realised that over-specification of the boundary fields was incorrect. In their seminal paper Charney, Fjørtoft, and von Neumann (1950) argued that, for the barotropic vorticity equation, two fields should be imposed at inflow and one at outflow. They imposed the stream function at all points and the vorticity at inflow points. Much later, Sundström (1969) proved that their choice of boundary conditions did, indeed, make the problem well-posed. In time, well-posed boundary conditions were derived for the linearized shallow water equations, Eulerian equations, and Navier-Stokes equations. See Oliger and Sundström (1978), who in the same paper point out that the Boussinesque and primitive equations are problematic; however, see Norbury and Cullen (1985).

Also from the very beginning, a second difficulty has plagued the numerical solution of the initial-boundary value problem: instability. It frustrated the above-mentioned Charney, Fjørtoft, and von Neumann (1950). As Platzman (1954) later showed, the extrapolation scheme they used at the outflow boundary was unstable. He showed that specifying all fields at all boundary points restores stability. Eventually, Gustafsson, Kreiss, and Sundström (1972) showed how to prove stability for the initial boundary value problem for discretized versions of the advection equation and the shallow water equation (in one dimension).

Despite these two difficulties being overcome, the dearth of well-posed meteorological models in the literature is striking. Elvius and Sundström (1973) have described and tested a well-posed shallow water model. As far as multi-level models are concerned no well-posed model has been documented to my knowledge. (Elvius (1977) and Mesinger (1977) have described primitive equation models which do not specify *every* field on the boundaries. Their boundaries are ‘fairly well-posed’). Flow relaxation schemes, (mainly for operational models) and radiation schemes (mainly for research models) totally dominate the literature; see McDonald (1997) for further discussion.

There is a third difficulty. A system can be well-posed and simultaneously reflect all waves from the boundary. (Well-posedness only guarantees that solutions will not amplify catastrophically). This is unsatisfactory: reflected gravity waves and/or sound waves may quickly contaminate the whole forecast area. The boundaries need to be *transparent* as well as well-posed. By transparent we mean that, first, all waves approaching the boundaries from the interior of the limited area should exit without reflection; and second, in a nested environment, where the boundary data are being supplied by a host model, all meteorologically important waves impinging on the boundaries from the exterior of the limited area should enter without their amplitude or phase being changed and without exciting spurious high frequency waves (noise). Engquist and Majda (1977) described a method for making the boundaries transparent to a clearly defined level of approximation. Their ideas have not been embraced with enthusiasm by the meteorological community. (There are exceptions; for example, Bourgeault, 1983, Klemp and Durran, 1983; Durran, et al., 1993; Lie, 2000, McDonald, 2002). Scientists in other disciplines, on the other hand, have followed up on these concepts and there now exist a variety of methods for making boundaries ‘as transparent as possible’. The literature is vast; see the reviews of Givoli (1992), and Tsynkov (1998).

Thus, a potential method for treating the boundaries which has a sound mathematical foundation which does not suffer from the weaknesses listed above for the flow relaxation scheme is available to meteorological modellers. In section 2 we examine the concepts involved in inventing transparent boundaries by applying them to one-dimensional equations which have a Meteorological flavour. In section 3 a hierarchy of transparent boundary conditions is derived for the shallow water equations. In section 4 some of these conditions are tested in a nested system and their effectiveness is compared with the more traditional relaxation boundary strategy. Finally, in section 5 the implication of the results obtained in section 4 is discussed.

## 2. THE BASIC CONCEPTS.

In this section the basic ideas involved in designing transparent boundary conditions are examined using one dimensional equations.

### 2.1 One-dimensional non-dispersive waves.

In this sub-section we use the one-dimensional shallow water equations to illustrate the underlying idea: we impose conditions at the artificial boundaries which enforce what our mathematical analysis tells us what would have happened anyway if the domain of integration had extended far beyond these artificial boundaries.

Consider the one-dimensional shallow water equations

$$\frac{\partial u(x, t)}{\partial t} + \bar{u} \frac{\partial u(x, t)}{\partial x} + \frac{\partial \Phi(x, t)}{\partial x} = 0, \quad (2.1)$$

$$\frac{\partial \Phi(x, t)}{\partial t} + \bar{u} \frac{\partial \Phi(x, t)}{\partial x} + \bar{\Phi} \frac{\partial u(x, t)}{\partial x} = 0, \quad (2.2)$$

where  $\bar{u}$  and  $\bar{\Phi}$  are constants. The notation is conventional. See appendix 1 for a list of the symbols not explicitly defined in the text. Substituting  $\Phi = \hat{\Phi} \exp i(kx - \omega t)$  yields a dispersion relation with two solutions:

$$\omega_+ = k(\bar{u} + \bar{c}); \quad \omega_- = k(\bar{u} - \bar{c}), \quad (2.3)$$

where  $\bar{c} = \sqrt{\bar{\Phi}}$ . Thus the following  $u$  and  $\Phi$  satisfy Eqs. (2.1) and (2.2):

$$u(x, t) = \frac{1}{\bar{c}} \left[ \hat{\Phi}_+ e^{ik[x - (\bar{u} + \bar{c})t]} - \hat{\Phi}_- e^{ik[x - (\bar{u} - \bar{c})t]} \right], \quad (2.4)$$

$$\Phi(x, t) = \hat{\Phi}_+ e^{ik[x - (\bar{u} + \bar{c})t]} + \hat{\Phi}_- e^{ik[x - (\bar{u} - \bar{c})t]}; \quad (2.5)$$

( $\hat{\Phi}_+$  and  $\hat{\Phi}_-$  are constants). In what follows we assume that  $\bar{c} > \bar{u}$  (The arguments are quite general, however) . Defining

$$p(x, t) = \Phi(x, t) + \bar{c}u(x, t); \quad q(x, t) = \Phi(x, t) - \bar{c}u(x, t), \quad (2.6)$$

we see that

$$p(x, t) = 2\hat{\Phi}_+ e^{ik[x - (\bar{u} + \bar{c})t]} \quad (2.7)$$

describes a wave travelling in the '+x' direction with a velocity  $\bar{u} + \bar{c}$ , and

$$q(x, t) = 2\hat{\Phi}_- e^{ik[x - (\bar{u} - \bar{c})t]} \quad (2.8)$$

describes a wave travelling in the '-x' direction with a velocity  $\bar{u} - \bar{c}$ .

If we are solving equations (2.1)-(2.2) over the range  $0 \leq x \leq L$  then for well-posedness, we must impose one field at  $x = 0$  and one field at  $x = L$  when  $\bar{c} > \bar{u}$ . See, for example, Elvius (1977). What choice of field will make the boundaries *transparent*? Consider the boundary at  $x = 0$ . We must impose one field and extrapolate the other. The  $\omega_+$ -wave will be approaching from the exterior. To make sure it enters the area accurately we impose the host model field which describes it:  $p^h(0, t)$ . (Looking from a meteorological perspective, and regarding these waves as noise, we impose  $p^h(0, t) = 0$ ). The  $\omega_-$ -wave will be approaching from the interior. If we extrapolate the other field carefully this wave can leave the area.

Consider the boundary at  $x = L$ . The  $\omega_-$ -wave will be approaching from the exterior. We would like it to enter accurately, which we do by imposing  $q^h(L, t)$ . (Again, from a meteorological viewpoint, these waves are noise, so we impose  $q^h(L, t) = 0$ ). If we extrapolate the other field judiciously the  $\omega_+$ -wave can leave the area.

To convince ourselves these arguments are correct let us integrate Eqs. (2.1)-(2.2), starting from the modulated wave:

$$\Phi(x, 0) = \hat{\Phi} \exp \left\{ - \left[ \frac{(x - L/2)}{(L/10)} \right]^2 \right\} \sin \left( \frac{16\pi x}{L} \right); \quad u(x, 0) = 0. \quad (2.9)$$

For our integration we choose  $L = 1000\text{km}$ ,  $\Delta x = 10\text{km}$ ,  $\Delta t = 25\text{s}$ ,  $\hat{\Phi} = 10$ ,  $\bar{c} = 300\text{m/s}$ , and  $\bar{u} = 0.0001\text{m/s}$ ; (this is to define inflow and outflow boundaries). For discretization details see McDonald (1999). The length of the integration,  $T$ , is 0.694444239hr.

The initial state is shown by the diamonds in figure 1. When we start the integration the wave packet will spread out, with one wave train moving in the ‘+ $x$ ’ direction at a velocity of 300m/s and another moving in the ‘- $x$ ’ direction at a velocity of -300m/s. If there were an infinite domain these waves would continue indefinitely. Therefore we would like our artificial boundary conditions to model this accurately. To see what can go wrong let us impose, first of all,  $\Phi = 0$  at  $x = 0$  and  $x = L$ . Looking at the dots in figure 1 we can see that the  $\omega_+$ -wave on reaching the boundary at  $x = L$  has been reflected back as an  $\omega_-$  wave. Its leading edge, which in an unbounded integration would have travelled +750km, has instead travelled +300km to  $x = L$ , has then been reflected and travelled -450km as an  $\omega_-$ -wave, ending up at  $x = 550\text{km}$ . The exact mirror of this phenomenon has occurred at  $x = 0$ . What happens if we impose  $p(0, t) = 0$  and  $q(L, t) = 0$ ? Then the waves exit without reflection as can be seen from figure 2.

## 2.2 One-dimensional dispersive waves.

In this subsection we use the one dimensional advection-adjustment equations to illustrate the complications caused by dispersive waves. The underlying idea is still valid: we perform a mathematical analysis to decide which waves are approaching the boundary. Then we impose boundary conditions to ‘help them on their way’ through the boundary. The presence of dispersion means that, although we can still invent local boundary conditions, they will be only approximately transparent; there will be some reflection of waves. In principle, we can make the reflection as small as we wish, but at a computational cost.

Complications arise when the waves are dispersive. To illustrate let us add Coriolis terms to Eqs. (2.1)-(2.2), giving us the one dimensional advection-adjustment equations:

$$\frac{\partial u(x, t)}{\partial t} + \bar{u} \frac{\partial u(x, t)}{\partial x} + \frac{\partial \Phi(x, t)}{\partial x} - \bar{f} v(x, t) = 0, \quad (2.10)$$

$$\frac{\partial v(x, t)}{\partial t} + \bar{u} \frac{\partial v(x, t)}{\partial x} + \bar{f} u(x, t) = 0, \quad (2.11)$$

$$\frac{\partial \Phi(x, t)}{\partial t} + \bar{u} \frac{\partial \Phi(x, t)}{\partial x} + \bar{\Phi} \frac{\partial u(x, t)}{\partial x} = 0, \quad (2.12)$$

where the Coriolis parameter  $\bar{f}$  is a constant.

Substituting  $(u, v, \Phi) = (\tilde{u}, \tilde{v}, \tilde{\Phi}) \exp i(kx - \omega t)$  yields a dispersion relation with three solutions; an advective and two dispersive adjustment solutions:

$$\omega_a = k\bar{u}; \quad \omega_+ = k(\bar{u} + c_k); \quad \omega_- = k(\bar{u} - c_k), \quad (2.13)$$

where

$$c_k = \sqrt{\bar{\Phi} + \bar{f}^2/k^2}, \quad (2.14)$$

yielding the following solutions to Eqs. (2.10)-(2.12);

$$u(x, t) = \int_{-\infty}^{\infty} dk \left\{ \frac{c_k}{\bar{\Phi}} \left[ \hat{\Phi}_+(k) e^{ik[x - (\bar{u} + c_k)t]} - \hat{\Phi}_-(k) e^{ik[x - (\bar{u} - c_k)t]} \right] \right\}, \quad (2.15)$$

$$v(x, t) = \int_{-\infty}^{\infty} dk \left\{ \frac{-i\bar{f}}{k\bar{\Phi}} \left[ \hat{\Phi}_+(k) e^{ik[x-(\bar{u}+c_k)t]} + \hat{\Phi}_-(k) e^{ik[x-(\bar{u}-c_k)t]} \right] + \frac{ik}{\bar{f}} \hat{\Phi}_a(k) e^{ik[x-\bar{u}t]} \right\}, \quad (2.16)$$

$$\Phi(x, t) = \int_{-\infty}^{\infty} dk \left\{ \hat{\Phi}_+(k) e^{ik[x-(\bar{u}+c_k)t]} + \hat{\Phi}_-(k) e^{ik[x-(\bar{u}-c_k)t]} + \hat{\Phi}_a(k) e^{ik[x-\bar{u}t]} \right\}. \quad (2.17)$$

Defining

$$u(x, t) = \int_{-\infty}^{\infty} dk e^{ikx} \hat{u}(k, t), \quad v(x, t) = \int_{-\infty}^{\infty} dk e^{ikx} \hat{v}(k, t),$$

$$\Phi(x, t) = \int_{-\infty}^{\infty} dk e^{ikx} \hat{\Phi}(k, t), \quad (2.18)$$

by inspection of Eqs. (2.15)-(2.17) we see that the following combination of  $\hat{v}$  and  $\hat{\Phi}$ , which we name  $\hat{B}_a$  for convenience, is a pure advective wave :

$$\hat{B}_a(k, t) = \hat{v}(k, t) + i \left( \frac{\bar{f}}{k\bar{c}} \right) \frac{\hat{\Phi}(k, t)}{\bar{c}} = i \left( \frac{\bar{f}}{k\bar{c}} \right)^{-1} \left( \frac{c_k}{\bar{c}} \right)^2 \frac{\hat{\Phi}_a}{\bar{c}} e^{-ik\bar{u}t}. \quad (2.19)$$

Also, the following combination of  $\hat{u}$ ,  $\hat{v}$  and  $\hat{\Phi}$ , which we name  $\hat{B}_+$  for convenience, is a pure  $\omega_+$ -wave

$$\hat{B}_+(k, t) = \frac{\hat{\Phi}(k, t)}{\bar{c}} + \hat{u}(k, t) \sqrt{1 + \left( \frac{\bar{f}}{k\bar{c}} \right)^2} + i \left( \frac{\bar{f}}{k\bar{c}} \right) \hat{v}(k, t); \quad \left[ = 2 \left( \frac{c_k}{\bar{c}} \right)^2 \frac{\hat{\Phi}_+}{\bar{c}} e^{-ik(\bar{u}+c_k)t} \right], \quad (2.20)$$

Lastly, the following is a pure  $\omega_-$ -wave, which we label  $\hat{B}_-$  :

$$\hat{B}_-(k, t) = \frac{\hat{\Phi}(k, t)}{\bar{c}} - \hat{u}(k, t) \sqrt{1 + \left( \frac{\bar{f}}{k\bar{c}} \right)^2} + i \left( \frac{\bar{f}}{k\bar{c}} \right) \hat{v}(k, t); \quad \left[ = 2 \left( \frac{c_k}{\bar{c}} \right)^2 \frac{\hat{\Phi}_-}{\bar{c}} e^{-ik(\bar{u}-c_k)t} \right]. \quad (2.21)$$

Consider

$$B_-^n(x, t) = \bar{c} \int_{-\infty}^{\infty} dk (ik)^n e^{ikx} \hat{B}_-(k, t); \quad \left[ = 2 \int_{-\infty}^{\infty} dk (ik)^n \left( \frac{c_k}{\bar{c}} \right)^2 \hat{\Phi}_- e^{ik[x-(\bar{u}-c_k)t]} \right]; \quad (2.22)$$

it describes an  $\omega_-$ -wave packet travelling in the ‘ $-x$ ’-direction when  $c_k > \bar{u}$ , exactly what we need to construct a transparent boundary, as we discussed in section (2.1). Unfortunately, the square-root term in  $\hat{B}_-(k, t)$  causes  $B_-^n(x, t)$  to be totally impracticable.

However, we can rescue the situation. If we expand the square root term in Eq. (2.21) using a Taylor expansion, assuming  $\bar{f}/k\bar{c} < 1$ , and then substitute  $\hat{B}_-(k, t)$  from Eq. (2.21) into Eq. (2.22) we can generate a hierarchy of transparent boundary conditions, using the definitions given in Eq. (2.18).

Dropping all the  $O(\bar{f}/k\bar{c})$  terms we recover the transparent boundary of section (2.1):

$$B_-^0(x, t) = \Phi(x, t) - \bar{c}u(x, t) \quad (2.23)$$

The next order of accuracy is obtained by keeping the  $O(\bar{f}/k\bar{c})$  terms in Eq. (2.21) and substituting  $\hat{B}_-(k, t)$  into Eq. (2.22):

$$B_-^1(x, t) = \frac{\partial \Phi(x, t)}{\partial x} - \bar{f}v(x, t) - \bar{c} \frac{\partial u(x, t)}{\partial x}. \quad (2.24)$$

The next order of accuracy is given by keeping the order  $(\bar{f}/k\bar{c})^2$  terms in Eq. (2.21) and substituting  $\hat{B}_-(k, t)$  into Eq. (2.22):

$$B_-^2(x, t) = \frac{\partial}{\partial x} \left( \frac{\partial \Phi(x, t)}{\partial x} - \bar{f}v(x, t) - \bar{c} \frac{\partial u(x, t)}{\partial x} \right) + \frac{\bar{f}^2}{2\bar{c}} u(x, t). \quad (2.25)$$

Next consider

$$B_+^n(x, t) = \bar{c} \int_{-\infty}^{\infty} dk (ik)^n e^{ikx} \hat{B}_+(k, t) = 2 \int_{-\infty}^{\infty} dk (ik)^n \left( \frac{c_k}{\bar{c}} \right)^2 \hat{\Phi}_+ e^{ik[x - (\bar{u} + c_k)t]}, \quad (2.26)$$

which describes an  $\omega_+$ -wave packet travelling in the ‘+ $x$ ’-direction when  $c_k > |\bar{u}|$ . This is what we need to construct a transparent boundary, as we discussed in section (2.1). As previously, we can generate a hierarchy of transparent boundary conditions:

$$B_+^0(x, t) = \Phi(x, t) + \bar{c}u(x, t) \quad (2.27)$$

$$B_+^1(x, t) = \frac{\partial \Phi(x, t)}{\partial x} - \bar{f}v(x, t) + \bar{c} \frac{\partial u(x, t)}{\partial x}, \quad (2.28)$$

$$B_+^2(x, t) = \frac{\partial}{\partial x} \left( \frac{\partial \Phi(x, t)}{\partial x} - \bar{f}v(x, t) + \bar{c} \frac{\partial u(x, t)}{\partial x} \right) - \frac{\bar{f}^2}{2\bar{c}} u(x, t). \quad (2.29)$$

Lastly, consider

$$B_a^n(x, t) = \int_{-\infty}^{\infty} dk (ik)^n e^{ikx} \hat{B}_a(k, t) = i \left( \frac{\bar{f}}{k\bar{c}} \right)^{-1} \int_{-\infty}^{\infty} dk (ik)^n \left( \frac{c_k}{\bar{c}} \right)^2 \frac{\hat{\Phi}_a}{\bar{c}} e^{ik[x - \bar{u}t]}; \quad (2.30)$$

it describes the advective wave packet travelling in the  $\bar{u}$ -direction, just what we need to construct a transparent boundary. To lowest order in  $(\bar{f}/k\bar{c})$ ,

$$B_a^0(x, t) = v(x, t) \quad (2.31)$$

describes an advective wave, and to next order

$$B_a^1(x, t) = \frac{\partial v(x, t)}{\partial x} - \frac{\bar{f}}{\bar{\Phi}} \Phi(x, t) \quad (2.32)$$

describes an advective wave. Looking at Eq. (2.19) we see that there are no higher order terms.  $B_a^1(x, t)$  is proportional to the one-dimensional linearized potential vorticity; recall that Charney (1962) proposed such a boundary condition for the barotropic primitive equations. Also,  $B_+^0, B_-^0$ , and  $B_a^0$  are the one-dimensional equivalent of the ‘case II’ boundary fields proposed by Elvius and Sundström (1973).

This derivation depends on  $\bar{f}/(k\bar{c})$  being small. In a meteorological context how valid is this? What would be a typical range of its values in the context of limited area meteorological modelling if we take  $\bar{f} = 10^{-4} s^{-1}$ ? For the external mode ( $\bar{c} \sim 300 \text{ms}^{-1}$ ) this coefficient is  $\leq 0.05$ , assuming the longest wavelength to be  $\sim 1000 \text{km}$ . The internal modes can have much smaller values of  $\bar{c}$ , of course. When the wavelength is  $1000 \text{km}$  and  $\bar{c} = 16 \text{ms}^{-1}$  then  $\bar{f}/(k\bar{c}) \sim 1$ . Therefore, if we are modelling over a  $1000 \text{km} \times 1000 \text{km}$  area  $\bar{f}/(k\bar{c}) \leq 1$  for the majority of modes, and most importantly,  $\bar{f}/(k\bar{c}) \ll 1$  for the

fast-moving short wavelength modes which we particularly do not want to be reflected from the boundaries. For smaller areas  $\bar{f}/(k\bar{c})$  will be even smaller.

If we are solving equations (2.10)-(2.12) over the range  $0 \leq x \leq L$ , then for well-posedness a field must be imposed on the boundary for each inward pointing characteristic; see, for example, Sundström and Elvius, 1979. Again, we restrict ourselves to  $\bar{c} > \bar{u}$ . Then we must impose two fields at  $x = 0$  and one at  $x = L$  when  $\bar{u} > 0$ , and two fields at  $x = L$  and one at  $x = 0$  when  $\bar{u} < 0$ .

What choice of field will make the boundaries *as transparent as possible*? Let us assume  $\bar{u} > 0$ . Consider the boundary at  $x = 0$ . The  $\omega_a$ - and  $\omega_+$ -waves will be approaching from the exterior. If we impose  $(B^h)_a^0$  and  $(B^h)_+^0$  we will be forcing the boundary with these waves, allowing them to enter with lowest order accuracy; (superscript  $h$  = host fields). Imposing  $(B^h)_+^1$  allows  $\omega_+$ -waves to enter with next order accuracy, while imposing  $(B^h)_a^1$  allows the advective wave to enter with full accuracy. We use  $(B^h)_+^2$  for even more accuracy, and so on. Simultaneously, we must extrapolate one other field to this boundary.

Consider the boundary at  $x = L$ . The only wave approaching from the exterior is the  $\omega_-$ -wave. To model it we impose the host model field which describes this wave:  $(B^h)_-^0$  for lowest order accuracy and  $(B^h)_-^1$  for next order accuracy, and so on. Simultaneously, we must extrapolate two other fields to this boundary.

To convince ourselves that our hierarchy of boundary conditions works let us integrate Eqs. (2.10)-(2.12). For our first test let us model an advective solution:

$$\Phi(x, t) = \check{\Phi} \exp \left[ - \left\{ \frac{(x - \bar{u}t - 3L/4)}{(L/10)} \right\}^2 \right] \quad (2.33)$$

$$v(x, t) = \frac{-2(x - \bar{u}t - 3L/4)}{\bar{f}(L/10)^2} \check{\Phi} \exp \left[ - \left\{ \frac{(x - \bar{u}t - 3L/4)}{(L/10)} \right\}^2 \right] \quad (2.34)$$

$$u(x, t) = 0, \quad (2.35)$$

which describes a geostrophically balanced bell initially centered at  $x = 3L/4$ , and subsequently moving without distortion with a velocity  $\bar{u}$ . We start from an initial state  $\Phi(x, 0)$ ,  $v(x, 0)$ , and  $u(x, 0)$ . For our integration we choose  $L = 1000\text{km}$ ,  $\Delta x = 10\text{km}$ ,  $\Delta t = 10\text{sec.}$ ,  $\bar{f} = 10^{-4}$ ,  $\bar{c} = 300\text{m/s}$ , and an advection velocity of  $\bar{u} = 100\text{m/s}$ . Details of the discretization are contained in McDonald (2000). We choose the length of the integration,  $T$ , such that the maximum of the bell will have moved to  $x = 5L/4$  after time  $T$ .

Because Eqs. (2.33)-(2.35) describe an advective solution, when we start the integration the balanced advective  $\Phi$ - and  $v$ - waves will move undistorted in the '+ $x$ ' direction with a velocity  $\bar{u} = 100\text{m/s}$ . With a transparent boundary at  $x = L$  these waves will exit without reflection. Since  $L\bar{f}/(20\pi\bar{c}) = 0.005$  the following zero order boundary condition should be extremely accurate: impose  $B_-^0(L, t) = \Phi(L, t) - \bar{c}u(L, t) = 0$ . At  $x = 0$  we impose  $p(0, t) = 0, v(0, t) = 0$ , which is essentially the analytical solution.

The outcome is shown in figure 3. The boundary is obviously highly reflective, and since the reflected wave is not in geostrophic balance ( $u \neq 0$ ), we conclude that an  $\omega_-$ -wave has been excited, which is confirmed by the position of the maximum of the reflected wave. It has travelled  $\sim -500\text{km} \sim (\bar{u} - c_k)T/2$  back from the boundary at  $x = L$ . Where has it all gone wrong? The answer is that  $B_-^0(L, t) = 0$  is an incorrect boundary condition

for a geostrophically balanced wave, because for such a wave  $\bar{f}v = \partial\Phi/\partial x$ , implying  $-i(\bar{f}/k\bar{c})\hat{v} = \hat{\Phi}/\bar{c}$ . Thus, the term in Eq. (2.21) which seems to be  $O(\bar{f}/k\bar{c})$  is, in fact,  $O(1)$ : we should have used  $B_-^1 = 0$ .

It is enlightening to look at what is happening in more detail. From Eqs. (2.15) and (2.17) we see that to  $O[(\bar{f}/k\bar{c})^2]$ ,  $\hat{\Phi} - \bar{c}\hat{u} = 2\hat{\Phi}_- \exp[-ik(\bar{u} - c_k)t] + \hat{\Phi}_a \exp[-ik\bar{u}t]$ . Thus, we were imposing an erroneous solution to this order when we imposed  $B_-^0 = 0$ . Since, to this order,  $\hat{\Phi} - \bar{c}\hat{u} + if\hat{v}/k = 2\hat{\Phi}_- \exp[-ik(\bar{u} - c_k)t]$ , imposing  $B_-^1 = 0$  kills the  $\omega_-$ -wave while leaving the other two almost unaffected.

So  $B_-^1 = 0$  should allow the advective wave to exit with miniscule reflection ( $(\bar{f}/k\bar{c})^2 \sim 0.25 \times 10^{-4}$ ). Repeating the test with this boundary condition, restores full transparency to the naked eye. (The forecast is not shown).

Before going on it is necessary to discuss the practical implementation of these boundary conditions. These pragmatic considerations are important because historically one of the main obstacles to progress has been the enormous difficulty involved in translating differential conditions into stable and accurate finite difference equations. In that light,  $B_-$  and  $B_+$ , as written in Eqs. (2.24), (2.25), (2.28), and (2.29) are unattractive for the following reasons. (a) They are difficult to install; in a semi-implicit system the  $\partial/\partial x$ -term feeds into the ‘Helmholtz equation’, which means that testing alternative discretizations is very tedious, becoming even more so for the higher order boundary conditions. (b) Because, for example, the condition  $B_-[L, (n+1)\Delta t] = 0$  involves all three fields at time level  $(n+1)$  it can only be solved iteratively. By substituting from Eqs. (2.10)-(2.12) we can generate more attractive alternatives, see appendix 2, two of which are listed in table 1. The ‘upstream boundary conditions’ avoid (a) and (b) above. They have the added attraction that they are very likely to be stable; see Gustafsson, Kreiss, and Sundström (1972). The ‘pure boundary conditions’ also avoid (a) above, but not (b).

	upstream boundary condition	pure boundary condition
$B_-^1$	$\frac{dq}{dt}$	$\frac{\partial q}{\partial t} + \bar{u}\bar{f}v$
$B_+^1$	$\frac{dp}{dt}$	$\frac{\partial p}{\partial t} + \bar{u}\bar{f}v$
$B_-^2$	$\frac{d}{dt} \left( \frac{\partial q}{\partial t} + (\bar{u} + \bar{c}) \frac{\partial q}{\partial x} \right)$	$\frac{\partial^2 q}{\partial t^2} + \bar{u}\bar{f} \frac{\partial v}{\partial t} + \frac{(\bar{u}^2 - \bar{c}^2)}{2\bar{c}} \bar{f}^2 u$
$B_+^2$	$\frac{d}{dt} \left( \frac{\partial p}{\partial t} + (\bar{u} - \bar{c}) \frac{\partial p}{\partial x} \right)$	$\frac{\partial^2 p}{\partial t^2} + \bar{u}\bar{f} \frac{\partial v}{\partial t} - \frac{(\bar{u}^2 - \bar{c}^2)}{2\bar{c}} \bar{f}^2 u$

TABLE 1. Alternative implementations of the boundary conditions  $B_-$  and  $B_+$ . In this table  $d/dt = \partial/\partial t + \bar{u}\partial/\partial x$

Next, let us try to demonstrate that the higher order boundary conditions are indeed more accurate than those of lower order. Since  $B_\pm^n$  contain no  $\hat{\Phi}_a$  terms for  $n > 1$  we cannot use advective waves for this test. Consider instead the following  $\omega_+$ -wave solution to Eqs. (2.10)-(2.12):

$$\begin{aligned} \Phi(x, t) &= \check{\Phi} \sin\left(\frac{2\pi}{L}[x - (\bar{u} + c_K)t]\right); & u(x, t) &= \check{\Phi} \frac{c_K}{\bar{\Phi}} \sin\left(\frac{2\pi}{L}[x - (\bar{u} + c_K)t]\right); \\ v(x, t) &= -\check{\Phi} \frac{L\bar{f}}{2\pi\bar{\Phi}} \cos\left(\frac{2\pi}{L}[x - (\bar{u} + c_K)t]\right); \end{aligned} \quad (2.36)$$

where  $c_K$  is given by Eq. (2.14) with  $k = 2\pi/L$ . We start our integration from an initial state  $\Phi(x, 0), u(x, 0)$  and  $v(x, 0)$ , and we impose  $v(0, t)$  and  $\Phi(0, t)$ , as given by Eq. (2.36). This combination models an  $\omega_+$ -wave of wavelength  $L$  moving in the positive  $x$  direction with a velocity  $\bar{u} + c_K$ . Choosing  $\bar{c} = 20\text{m/s}$  means that  $\bar{f}/(\bar{c}k) = 0.796$ ; thus if we use  $B_-^1(L, t) = 0$  as the boundary condition we expect some reflection. We see this in figure 4, where  $(\Phi + \bar{\Phi}u/\bar{c}_K)/2$  and  $(\Phi - \bar{\Phi}u/\bar{c}_K)/2$  have been plotted in order to highlight the reflected wave.

(I have chosen  $\bar{u} = 5\text{m/s}$ , and the duration of the integration  $T = 9.08964729\text{hr}$ , exactly equal to the time it takes the  $\omega_+$ -wave to move a distance  $L = 1000\text{km}$ . Thus if there were no reflection the waves at time  $T$  in figure 4 would exactly overlap the initial wave). Notice that the leading edge of the reflected wave has travelled  $\sim 500\text{km}$  and its dominant wavelength is  $\sim 500\text{km}$ , both of which are consistent with an  $\omega_-$ -wave travelling with a velocity of  $\bar{u} - c_{k_-} \sim -16.5\text{m/s}$

I have used the ‘upstream boundary’ condition  $B_-^1$  from table 1 for the integration displayed in figure 4; the ‘pure boundary condition’ gives the same result (not shown).

Will  $B_-^2$  reduce the reflection? The answer is yes, provided we are very careful. Consider the ‘pure boundary condition’  $B_-^2$  from table 1. It is a second order equation, and as such requires two initial conditions;  $q(L, 0)$  and  $\partial q(L, 0)/\partial t$ . If we supply *accurate* values of these quantities and impose  $B_-^2(L, t) = 0$  we get the forecast shown in figure 5. Notice the reflection has been significantly reduced.

If we do not supply an accurate value of  $\partial q(L, 0)/\partial t$ , but instead use the erroneous value which is ‘natural’ when we discretize in time,  $q(L, -\Delta t) = q(L, 0)$ , then *the reflection at the boundary is just as large as if we had used  $B_-^1(L, t) = 0$* ; see figure 6. Thus, the whole integration is dominated by this single datum. We return to this issue later when we discuss the strengths and weaknesses of these boundary options.

### 3. EXTENSION TO TWO DIMENSIONS.

The approach used in section 2 for deriving approximately transparent boundary conditions in one dimension can easily be extended to the two-dimensional shallow water equations; see McDonald (2002). It has a number of attractions: the derivation is simple; we can maintain an intuitive understanding of what is happening because meteorologically familiar fields such as vorticity, divergence, and geostrophically balanced combinations of fields naturally emerge from the derivation. However, in the mathematical literature a slightly different approach is used to arrive at essentially the same results. Since a large body of the literature on non-reflecting boundaries, which we would like to use for guidance, pre-supposes familiarity with this approach let us use it to extend the derivation of approximately transparent boundary conditions to the two-dimensional linearized shallow water equations in this section.

The seminal paper is that of Engquist and Majda (1977). In this section we sketch their approach. See also Wagatha (1983) and Lie (2000).

The linearized shallow water equations are as follows.

$$\frac{\partial u}{\partial t} + \bar{u}\frac{\partial u}{\partial x} + \bar{v}\frac{\partial u}{\partial y} + \frac{\partial \Phi}{\partial x} - \bar{f}v = 0, \quad (3.1)$$

$$\frac{\partial v}{\partial t} + \bar{u}\frac{\partial v}{\partial x} + \bar{v}\frac{\partial v}{\partial y} + \frac{\partial \Phi}{\partial y} + \bar{f}u = 0, \quad (3.2)$$

$$\frac{\partial \Phi}{\partial t} + \bar{u} \frac{\partial \Phi}{\partial x} + \bar{v} \frac{\partial \Phi}{\partial y} + \bar{\Phi} \left( \frac{\partial u}{\partial x} + \frac{\partial v}{\partial y} \right) = 0. \quad (3.3)$$

The  $x$  and  $y$  components of the winds are  $u$  and  $v$  and  $\Phi = gz$  is the geopotential height. The Coriolis parameter,  $\bar{f}$ , the advecting velocities,  $\bar{u}$ , and  $\bar{v}$ , and  $\bar{\Phi}$ , the mean geopotential height, are all constants. Re-arrangement gives

$$\frac{\partial v}{\partial x} + \frac{1}{\bar{u}} \left[ \left( \frac{\partial}{\partial t} + \bar{v} \frac{\partial}{\partial y} \right) v + \frac{1}{2} \left( \bar{f} + \sqrt{\bar{\Phi}} \frac{\partial}{\partial y} \right) \left( u + \frac{\Phi}{\sqrt{\bar{\Phi}}} \right) + \frac{1}{2} \left( \bar{f} - \sqrt{\bar{\Phi}} \frac{\partial}{\partial y} \right) \left( u - \frac{\Phi}{\sqrt{\bar{\Phi}}} \right) \right] = 0, \quad (3.4)$$

$$\frac{\partial}{\partial x} \left( u + \frac{\Phi}{\sqrt{\bar{\Phi}}} \right) + \frac{1}{\bar{u} + \sqrt{\bar{\Phi}}} \left[ \left( \frac{\partial}{\partial t} + \bar{v} \frac{\partial}{\partial y} \right) \left( u + \frac{\Phi}{\sqrt{\bar{\Phi}}} \right) - \left( \bar{f} - \sqrt{\bar{\Phi}} \frac{\partial}{\partial y} \right) v \right] = 0, \quad (3.5)$$

$$\frac{\partial}{\partial x} \left( u - \frac{\Phi}{\sqrt{\bar{\Phi}}} \right) + \frac{1}{\bar{u} - \sqrt{\bar{\Phi}}} \left[ \left( \frac{\partial}{\partial t} + \bar{v} \frac{\partial}{\partial y} \right) \left( u - \frac{\Phi}{\sqrt{\bar{\Phi}}} \right) - \left( \bar{f} + \sqrt{\bar{\Phi}} \frac{\partial}{\partial y} \right) v \right] = 0. \quad (3.6)$$

If for each of the fields we make the substitution

$$\Psi(x, y, t) = \frac{1}{2\pi} \int_{-\infty}^{\infty} dl e^{ily} \int_{-\infty}^{\infty} d\omega e^{-i\omega t} \hat{\Psi}(x, l, \omega), \quad (3.7)$$

then a little algebra yields the following for the Fourier components:

$$\frac{\partial}{\partial x} \begin{bmatrix} \hat{v} \\ \hat{u} + \frac{\hat{\Phi}}{\sqrt{\bar{\Phi}}} \\ \hat{u} - \frac{\hat{\Phi}}{\sqrt{\bar{\Phi}}} \end{bmatrix} = -i(-\omega + l\bar{v}) \begin{bmatrix} \frac{1}{\bar{u}} & \frac{f_-}{2\bar{u}} & \frac{-f_+}{2\bar{u}} \\ \frac{f_+}{\bar{u} + \sqrt{\bar{\Phi}}} & \frac{1}{\bar{u} + \sqrt{\bar{\Phi}}} & 0 \\ \frac{-f_-}{\bar{u} - \sqrt{\bar{\Phi}}} & 0 & \frac{1}{\bar{u} - \sqrt{\bar{\Phi}}} \end{bmatrix} \begin{bmatrix} \hat{v} \\ \hat{u} + \frac{\hat{\Phi}}{\sqrt{\bar{\Phi}}} \\ \hat{u} - \frac{\hat{\Phi}}{\sqrt{\bar{\Phi}}} \end{bmatrix}, \quad (3.8)$$

where

$$f_{\pm} = \frac{l\sqrt{\bar{\Phi}} \pm i\bar{f}}{-\omega + l\bar{v}} \quad (3.9)$$

Let us write Eq. (3.8) in the symbolic form in order to see where we are headed:

$$\frac{\partial}{\partial x} \hat{\Psi}(x, l, \omega) = i\mathbf{M}(l, \omega) \hat{\Psi}(x, l, \omega). \quad (3.10)$$

Comparing Eqs.(3.8) and (3.10) the definitions of  $\hat{\Psi}$  and  $\mathbf{M}$  are transparent. Multiply by a matrix  $\mathbf{V}(l, \omega)$  which diagonalizes  $\mathbf{M}$  and we get

$$\frac{\partial}{\partial x} \mathbf{V}(l, \omega) \hat{\Psi}(x, l, \omega) = i\mathbf{\Lambda}(l, \omega) \mathbf{V}(l, \omega) \hat{\Psi}(x, l, \omega) \quad (3.11)$$

where  $\mathbf{\Lambda}(l, \omega) = \mathbf{V}(l, \omega) \mathbf{M}(l, \omega) \mathbf{V}^{-1}(l, \omega)$  is a diagonal matrix. By defining  $\hat{\mathbf{w}} = \mathbf{V} \hat{\Psi}$  we can write Eq. (3.11) as

$$\frac{\partial}{\partial x} \hat{\mathbf{w}}(x, l, \omega) = i\mathbf{\Lambda}(l, \omega) \hat{\mathbf{w}}(x, l, \omega), \quad (3.12)$$

and it has the solutions

$$\hat{w}_j(x, l, \omega) = \tilde{w}_j(l, \omega) e^{ik_j(l, \omega)x} ; \quad j = 1, 2, 3. \quad (3.13)$$

where  $k_j = \Lambda_{jj}$ . Substituting for  $\hat{w}$  and multiplying by  $\exp i(l y - \omega t)$  we get,

$$[\mathbf{V}(l, \omega) \hat{\Psi}(x, l, \omega)]_j e^{i l y - i \omega t} = \tilde{w}_j(l, \omega) e^{i(k_j x + l y - \omega t)} \quad (3.14)$$

Recall the procedure for diagonalizing a matrix. First, find the eigenvalues:  $k_j$ . Then the diagonalizing matrix,  $\mathbf{V}$ , consists of the left eigenvectors associated with these eigenvalues. Thus, computing the eigenvalues,  $k_j$ , enables us to select a particular wave, and by looking at the exponential on the right hand side of Eq. (3.14) we can decide the direction in which it is travelling. In addition, computing  $\mathbf{V}$  enables us to project out that uni-directional wave in the transformed system. Now, if we can express  $\mathbf{V}(l, \omega)$  as a polynomial in  $l$  and  $\omega$  then when we transform back to physical space we will have a polynomial in  $\partial/\partial y$  and  $\partial/\partial t$ . Therefore, we have a formalism for generating a unidirectional wave equation. We can impose it on the boundary to transport the waves associated with  $k_j$  out of the area.

This is the fundamental idea, and although we have discussed it in terms of the linearized shallow water equation it is also appropriate for applying to other equations, for instance, the linearized Euler or Navier-Stokes equations. Let us now see how it works in practice for the shallow water system, for which

$$\mathbf{V} = \begin{bmatrix} 1 & \frac{1}{2} \left( \frac{\bar{u}}{\bar{\Phi}} + 1 \right) f_- & \frac{1}{2} \left( \frac{\bar{u}}{\bar{\Phi}} - 1 \right) f_+ \\ -\frac{\bar{u}}{\sqrt{\bar{\Phi}}} f_+ & 1 - \frac{1}{2} (1 - Y) & \frac{1}{2} (1 - Y) \frac{f_+}{f_-} \\ -\frac{\bar{u}}{\sqrt{\bar{\Phi}}} f_- & \frac{1}{2} (1 - Y) \frac{f_-}{f_+} & 1 - \frac{1}{2} (1 - Y) \end{bmatrix} \quad (3.15)$$

where

$$Y = \left[ 1 + f_+ f_- \left( \frac{\bar{u}^2}{\bar{\Phi}^2} - 1 \right) \right]^{\frac{1}{2}}. \quad (3.16)$$

In Eq. (3.15) the arbitrary normalization factor for each of the left eigenvectors as been chosen such that the leading terms on the diagonal are  $O(1)$ . (Computing the eigenvalues and left eigenvectors of  $\mathbf{M}$  is straightforward but tedious. If the reader is interested in the details I will happily provide a copy of my own derivation).

One of the eigenvalues,  $k_1$ , is associated with the advection wave, and the other two,  $k_2$  and  $k_3$ , with the adjustment waves. Let us examine the advective solution first. For it,

$$k_1 = \frac{1}{\bar{u}} (\omega - l \bar{v}), \quad (3.17)$$

and computing the left eigenvector associated with the eigenvalue  $k_1$  gives us, up to an arbitrary normalization,

$$\hat{B}_1(x, l, \omega) = \left( -\frac{l \bar{u}}{\omega} + \frac{i \bar{f}}{\omega} \right) \hat{u} + \left( 1 - \frac{l \bar{v}}{\omega} \right) \hat{v} + \left( -\frac{l \sqrt{\bar{\Phi}}}{\omega} + \frac{i \bar{f}}{\omega} \frac{\bar{u}}{\sqrt{\bar{\Phi}}} \right) \frac{\hat{\Phi}}{\sqrt{\bar{\Phi}}} \quad (3.18)$$

Substituting  $\omega$  from Eq. (3.17) in the exponentiated factor on the right hand side of Eq. (3.14) yields

$$e^{i(k_1 x + l y - \omega t)} = e^{i[k_1(x - \bar{u}t) + l(y - \bar{v}t)]}, \quad (3.19)$$

a wave travelling in the same direction as the  $x$ -component of the advecting velocity.

Looking at Eq. (3.18) we see that for small enough  $l$  and  $\bar{f}$  the advective wave is dominated by  $v$ . Dropping all the  $O(\omega^{-1})$  terms and transforming back let us call the result  $B_1^0$  :

$$B_1^0(x, y, t) = v(x, y, t) \quad (3.20)$$

Multiplying Eq. (3.18) by  $-i\omega$  and transforming back let us call the result  $B_1^1$ :

$$B_1^1(x, y, t) = \frac{\partial v}{\partial t} + \bar{v} \frac{\partial v}{\partial y} + \frac{\partial \Phi}{\partial y} + \bar{f}u + \bar{u} \left( \frac{\partial u}{\partial y} + \frac{\bar{f}}{\bar{\Phi}} \Phi \right), \quad (3.21)$$

Substituting from Eq. (3.2) we are back on familiar territory;  $B_1^1$  is proportional to the potential vorticity:

$$B_1^1(x, y, t) = -\bar{u} \left( \frac{\partial v}{\partial x} - \frac{\partial u}{\partial y} - \frac{\bar{f}}{\bar{\Phi}} \Phi \right) \quad (3.22)$$

We can, of course, see directly from Eqs. (3.1)-(3.3) that this combination of fields is an advective solution since  $dB_1^1/dt = 0$ .

There is no approximation;  $B_1^1$  projects out the advection wave accurately, independent of the size of  $l$  and  $\bar{f}$ . For the adjustment waves, on the other hand, we must resort to approximation. Their eigenvalues can be written as

$$k_{\pm 3} = \frac{\omega}{\bar{u} \pm \sqrt{\bar{\Phi}}} \left( 1 - \frac{l\bar{v}}{\omega} \right) \left[ 1 \pm \frac{\sqrt{\bar{\Phi}}}{\bar{u} \mp \sqrt{\bar{\Phi}}} (1 - \sqrt{1 + \epsilon_\omega}) \right] \quad (3.23)$$

where  $\epsilon_\omega$  contains only higher order terms:

$$\epsilon_\omega = \left( \frac{\bar{u}^2}{\bar{\Phi}} - 1 \right) \left( \frac{f^2}{\omega^2} + \frac{\bar{\Phi}l^2}{\omega^2} \right) \left( 1 - \frac{l\bar{v}}{\omega} \right)^{-2} \quad (3.24)$$

Ignoring the  $O(\omega^{-2})$  terms we can see by substituting  $\omega$  from Eq. (3.23) in the exponentiated factor on the right hand side of Eq. (3.14) that (for printing convenience  $k_+ = k_2; k_- = k_3$ )

$$e^{i(k_\pm x + l y - \omega t)} = e^{ik_\pm [x - (\bar{u} \pm \sqrt{\bar{\Phi}})t] + i l (y - \bar{v}t)}, \quad (3.25)$$

enabling us to determine the direction in which the wave is travelling.

From Eq. (3.15) we can write

$$(\mathbf{V}\hat{\Psi})_{\pm 3} = \left( \hat{u} \pm \frac{\hat{\Phi}}{\sqrt{\bar{\Phi}}} \right) - \frac{\bar{u}}{\sqrt{\bar{\Phi}}} f_\pm \hat{v} - \frac{1}{2}(1 - Y) \left[ \left( 1 - \frac{f_\pm}{f_\mp} \right) \hat{u} \pm \left( 1 + \frac{f_\pm}{f_\mp} \right) \frac{\hat{\Phi}}{\sqrt{\bar{\Phi}}} \right] \quad (3.26)$$

Of these terms,  $f_\pm$  is  $O(1/\omega)$  and  $1 - Y$  is  $O(1/\omega^2)$ . Let us assume it is legitimate to drop all the higher order terms and to transform back. Calling the result  $B^0$ , we see that, to lowest order, the  $k_2$  and  $k_3$ -waves are dominated by the characteristic variables:

$$B_{\pm 3}^0(x, y, t) = u(x, y, t) \pm \frac{1}{\sqrt{\bar{\Phi}}} \Phi(x, y, t) \quad (3.27)$$

$B_1^0, B_2^0$ , and  $B_3^0$  are the ‘case II’ boundary fields proposed by Elvius and Sundström (1973).

If we keep the terms up to  $O(1/\omega)$  in Eq. (3.26), then multiply by  $i(-\omega + l\bar{v})$  and transform back, calling the result  $B^1$  we get a more accurate projection of the  $k_2$  and  $k_3$ -waves:

$$B_{\frac{2}{3}}^1(x, y, t) = \left( \frac{\partial}{\partial t} + \bar{v} \frac{\partial}{\partial y} \right) \left( u \pm \frac{\Phi}{\sqrt{\Phi}} \right) \pm \frac{\bar{u}}{\sqrt{\Phi}} \left( \bar{f} \mp \sqrt{\Phi} \frac{\partial}{\partial y} \right) v, \quad (3.28)$$

We can gain some physical insight by substituting from Eqs. (3.5) and (3.6):

$$B_{\frac{2}{3}}^1(x, y, t) = -(\bar{u} \pm \sqrt{\Phi}) \left[ \left( \frac{\partial u}{\partial x} + \frac{\partial v}{\partial y} \right) \pm \frac{1}{\sqrt{\Phi}} \left( \frac{\partial \Phi}{\partial x} - \bar{f} v \right) \right], \quad (3.29)$$

which is identically zero for geostrophically balanced fields. Also, from Eqs. (3.5) and (3.6) we can generate a conditions which is attractive in terms of a semi-Lagrangian implementation:

$$B_{\frac{2}{3}}^1(x, y, t) = (\bar{u} \pm \sqrt{\Phi}) \frac{d}{dt} (\Phi \pm \sqrt{\Phi} u). \quad (3.30)$$

This boundary condition has been discussed and tested extensively in McDonald (2002), and we will subject it and Eq. (3.27) to a more severe test in section 4.

We can project out higher order equations for the adjustment modes by expanding  $1 - Y$ . It is more appropriate to use a Padé approximation rather than a Taylor expansion for the square root; see Engquist and Majda (1977).

#### 4. NUMERICAL TESTING.

In this section are described the testing of some of the boundary options examined in section 3, and the comparison of their effectiveness with the well-established relaxation scheme of Davies (1976) and Källberg (1977).

Promising results were obtained by McDonald (2002) for the *linearized* system of equations (2.10)-(2.12) using imposed *analytical* boundary fields. Here we inject more operational realism into our tests in two ways: we restore the non-linear terms in the shallow water equations, and we impose pseudo-operational boundary fields. Holstad and Lie (2001) have also tested these equations using a finite element formulation.

Thus we solve the equations

$$\frac{du}{dt} + \frac{1}{a \cos \theta} \frac{\partial \Phi}{\partial \lambda} - \left( f + \frac{u \tan \theta}{a} \right) v = 0, \quad (4.1)$$

$$\frac{dv}{dt} + \frac{1}{a} \frac{\partial \Phi}{\partial \theta} + \left( f + \frac{u \tan \theta}{a} \right) u = 0, \quad (4.2)$$

$$\frac{d\Phi}{dt} + \frac{\Phi}{a \cos \theta} \left( \frac{\partial u}{\partial \lambda} + \frac{\partial v \cos \theta}{\partial \theta} \right) = 0 \quad (4.3)$$

where

$$\frac{d}{dt} = \frac{\partial}{\partial t} + \frac{u}{a \cos \theta} \frac{\partial}{\partial \lambda} + \frac{v}{a} \frac{\partial}{\partial \theta}. \quad (4.4)$$

The notation is conventional; the symbols are defined in appendix 1. The Coriolis parameter becomes  $f = 2\Omega(\cos\theta_0 \sin\theta + \sin\theta_0 \cos\theta \cos\lambda)$  if we shift the pole by an angle  $\theta_0$ .

To test our boundary strategies we follow the suggestion of Baumhefner and Perkey (1982): we use a large area host model integration to generate the boundary fields for a smaller guest area which is nested within the host area. The large area fine grid forecast defines the ‘correct answer’ which the the guest area fine grid forecast strives to attain. The large area coarse grid forecast furnishes the boundary fields for the guest area integration.

The experimental set-up is as follows. The host area is horizontally discretized in two different configurations on a rotated latitude-longitude grid for which  $\theta_0 = 60^\circ$ . The fine mesh contains  $202 \times 178$  points with  $\Delta\lambda = \Delta\theta = 0.4^\circ$ . The coarse mesh contains  $68 \times 60$  points with  $\Delta\lambda = \Delta\theta = 1.2^\circ$ , for which every third point coincides with a fine mesh point.

The guest area consists of  $60 \times 60$  mesh points which coincide with the following host area fine grid points: (72  $\rightarrow$  131) in the east-west direction, and (60  $\rightarrow$  119) in the north-south direction. In round numbers the host area is  $9000km \times 8000km$  and the guest area is  $2500km \times 2500km$

To generate a ‘correct forecast’ the shallow water equations are integrated for 48h on the fine grid over the host area using a time step of 10min. All fields are stored at every time step at every grid point over the guest area. This data set represents the ‘correct forecast’. To generate ‘coarse’ boundary fields for the guest area the procedure is repeated on the coarse grid. (This data set also represents the worst case scenario for the guest forecasts. If they do not beat the coarse mesh host forecasts they are failures.)

The forecasts are verified over a central area consisting of the following  $20 \times 20$  grid points of the guest area: points (21  $\rightarrow$  40) in the east-west direction, and points (21  $\rightarrow$  40) in the north-south direction. All forecasts are verified against the host model fine mesh forecast.

The fine grid starting analysis for the host area consists of a set of 500hPa height and wind fields. These are interpolated from an analysis performed using the optimal interpolation analysis of the HIRLAM, ( Källén, 1996), which uses hybrid coordinates in the vertical. As a result, the wind and height fields are not in balance. To correct this a digital filter initialization (Lynch, 1996) is performed. The host area coarse grid starting analysis consists of the fields defined at every third point of the fine grid analysis.

The guest area starting fields derive from the initialized host area fine grid fields without interpolation, since the grids coincide.

In an operational context the fields from the host area coarse integration are available only intermittently to the guest model. To model this the fields from the coarse mesh integration are supplied to the guest model boundaries at intervals which are multiples of the time step: at times  $m\Delta t, 2m\Delta t, 3m\Delta t$ , and so on. The following linear interpolation is performed to generate these fields at each time step,  $n\Delta t$ , between time steps  $pm\Delta t$  and  $(p + 1)m\Delta t$ .

$$\psi[(n + pm)\Delta t] = \psi[pm\Delta t] + \frac{n}{m} \{ \psi[(p + 1)m\Delta t] - \psi[pm\Delta t] \} \quad (4.5)$$

In the tests described below the time step  $\Delta t = 10\text{min}$ , and the refreshment interval is 3h; thus  $m = 18$ .

We discretize Eqs. (4.1)-(4.4) in a semi-Lagrangian fashion. The details are given in McDonald (2002). Minor modifications are needed to take account of the non-linearity. The non-linear terms are evaluated half way along the trajectory as described in McDonald

and Haugen (1992). Also,  $\Phi_0$ , the linearizing geopotential height value, is chosen as the maximum value of  $\Phi$ .

In order to compare the new boundary strategies with that used operationally in the HIRLAM an ‘passive buffer zone’ of two lines external to the boundary line is used in the guest model integrations. Thus, in the East-West direction all the fields on lines 1, 2, 59 and 60 are refreshed using Eq. (4.5). Lines 3 and 57 are the boundary lines. The same applies in the North-South direction.

We will test 5 boundary strategies, three of which are ‘well specified’ in the sense that we impose two two fields at inflow and one at outflow.

Strategy (i). On the boundary line impose  $\Phi$  at all points and  $v_T$  at the inflow points. Let us call this call this ‘ $\Phi$  b.c.’.

Strategy (ii). On the boundary line impose  $\Phi - \sqrt{\Phi_0}v_N$  at all points and  $v_T$  at the inflow points. Let us call this call this ‘characteristic b.c.’.

Strategy (iii). Impose  $\Phi - \sqrt{\Phi_0}v_N$  and  $v_T$  at the inflow points and impose  $d(\Phi - \sqrt{\Phi_0}v_N)/dt$  at the outflow points on the boundary line, as we derived in Eq. (3.30). Let us call this ‘semi-transparent b.c.’.

It must be emphasised that no field from the passive buffer zone is used in any of the well specified strategies. Fields external to the boundary line are always estimated by extrapolation from the interior. In the final two boundary strategies the fields in the passive buffer zone are always used when needed. No extrapolations from the interior are performed.

Strategy (iv). On the boundary line impose  $\Phi$  and  $v_T$  at all points, and use the fields in the passive buffer zone whenever needed. Let us call this call this ‘S.L.b.c.’.

Strategy (v). This boundary treatment consists of strategy (iv) plus relaxation of the fields toward the host model fields in the relaxation zone. Lines 3-10 and lines 50-57 in both the East-West and North-South directions define the relaxation zone. The relaxation coefficients are 1.0, 0.962, 0.854, 0.691, 0.500, 0.309, 0.146, 0.038. Let us call this call this ‘relaxation b.c.’.

Let us look at four aspects of the integrations to judge the quality of our boundary strategies. First we look at the behaviour of the absolute value of the divergence,  $|\overline{D}|$ , averaged over the guest integration area. This is a good measure of whether the integration is well-balanced. Large values of  $|\overline{D}|$  indicate a surplus gravity-inertia waves. Increasing  $|\overline{D}|$  is a sign of an instability. Second, we will plot the evolution of  $\Phi$  averaged over the integration area to measure mass conservation. If the mass mis-behaves then our boundary strategy is flawed. Third, and fourth, and most importantly, we will plot the evolution of the rms wind and height errors for our verification area, using the host model fine mesh forecast as the ‘correct forecast’.

In figure 7  $|\overline{D}|$  multiplied by  $10^8$  is displayed. For all five boundary strategies it is similar in size to that of the correct forecast and not increasing as the forecast proceeds. We can infer that the forecasts are stable and balanced.

Comparing the mass evolution with the correct answer, see figure 8, we see that the ‘semi-transparent b.c.’ forecast exhibits strange behaviour from 18h onwards. For the other boundary strategies the mass is well behaved, though not exactly conserved.

The wind errors are shown in figure 9. The boundary strategies called ‘ $\Phi$  b.c.’ and ‘semi-transparent b.c.’ exhibit skill out to approximately 24h. The other three have skill

out to approximately 30h. Subsequently, all except ‘ $\Phi$  b.c.’ agree approximately with the host model coarse mesh forecast verified over the same area. This latter behaviour is reasonable since the distance from the boundary to the centre of the area is approximately 1200km. To travel this distance in 24h one must move at a speed of 14m/s, a modest advection speed. Thus it is not surprising that the forecast from 24h onwards is dictated by the boundaries. Of the five boundary strategies ‘ $\Phi$  b.c.’ is a clear loser. Up until the asymptotic solution is reached ‘characteristic b.c.’ looks best overall, and ‘relaxation b.c.’ is worst in the 9h to 18h forecast period; ‘semi-transparent b.c.’ shows no advantage over ‘characteristic b.c.’, and ‘S.L. b.c.’ is quite competitive after an initial ‘error shock’.

This ‘error shock’ at the start of the forecast is more pronounced in the wind errors; see figure 10. It develops in about 1.5h to 3h, depending on the boundary strategy. A time of 1.5 hours is consistent with a gravity wave of speed  $\sqrt{\Phi_0} = 241\text{m/s}$  travelling 1200km from the boundary to the centre of the area. Baumhefner and Perkey (1982) saw a similar, but much more severe effect: ‘forecasts made by the unbounded coarse mesh model are more accurate than the limited area fine mesh model early in the forecast’. They explained this effect as being due to the ‘excitation of rapidly moving spurious waves’. It was also seen by Holstad and Lie (2001) who reduced it by symmetrizing the original PDE system. Subsequent to the shock ‘semi-transparent b.c.’ shows essentially no skill. The strategy called ‘ $\Phi$  b.c.’ has some skill out to about 18h, but subsequent to that shows suspect behaviour. The other 3 boundary strategies show some skill out to between 18h and 30h, with ‘characteristic b.c.’ again being best.

We may speculate that ‘error shock’ displayed in figure 10 comes from some residual imbalance in the fields. We can re-enforce this opinion by repeating the experiments described above, but now using uninitialized data. The result (not shown) is that all of the forecasts for all boundary strategies, although stable, have essentially no skill.

## 5. DISCUSSION.

In a meteorological context, non-linear effects are of primary importance. However, the analysis which leads to transparent boundary conditions is based on the *linearized* shallow water equations. Thus an important question has not been addressed by this analysis: will the non-linear terms cause explosive growth at the boundary? For instance, Olinger and Sundström (1978), point out that ‘the important case where velocities change sign on the on the boundary and do not vanish in a neighbourhood of such a boundary point is not covered by existing theory’. Given this weakness in our theoretical guidance it is essential that we test these schemes using non-linear equations in simplified systems rather than trusting the analysis and experiments with linear systems to provide sufficient encouragement to jump straight to multi-level models. The results of section 4 reinforce this opinion. Although we saw no evidence of instability, neither did we find unambiguous confirmation of a hierarchy of enhanced accuracy we expected based on our derivations in section 3.

As so often happens, expectations raised by tests performed on linear systems (McDonald, 2002) have to be lowered when these tests are repeated in the more challenging non-linear environment. Looking at figures 8, 9 and 10 the following interpretation is reasonably fair. The boundary strategy called ‘characteristic b.c.’ is the best. Interestingly, the next best is ‘S.L.b.c.’. Both beat the ‘relaxation b.c.’, which corresponds

to our operational HIRLAM boundary treatment. The strategy called ‘ $\Phi$  b.c.’ behaves unacceptably. We had expectations from our analysis in section 3 that ‘semi-transparent b.c.’ would be superior to ‘characteristic b.c.’; in fact, the former is disconcertingly badly behaved. Holstad and Lie (2001) also found the ‘semi-transparent b.c.’ to be inferior. We can only speculate that our analysis, which included neither non-linear effects nor Rossby waves, gives poor guidance for the full equations.

Since ‘S.L.b.c.’ is simply ‘relaxation b.c.’ with the relaxation switched off we can see the errors induced by the relaxation procedure in figure 9 in particular. Thus, we *can* improve our forecasts if we can invent a better boundary strategy. However, a number of issues need to be resolved before we even consider testing ‘characteristic .b.c.’, the best boundary strategy, in a multi-level model.

The first question is: is it robust? We can partially answer this question by including orography in the shallow water model. The second question is: what is causing the ‘error shock’ seen in the height errors, and how can we eliminate it?

In an operational meteorological context the imposed boundary fields will always contain errors. We would like to separate these into ‘unavoidable’ and ‘potentially avoidable’ errors. The source of the unavoidable errors is the fact that the host model supplies *forecast* fields whose accuracy, by definition, deteriorates as the forecast proceeds. The source of the potentially avoidable errors is the incompatibility of the host and guest models (caused by different grids, orography, physics, etc. ). This can result in the imposed fields being ‘out of balance’, giving rise to ‘noise’, which may amplify and corrupt the forecast in the nested area. As we discussed in section 4 an essential preliminary step is to initialize both the host and guest models. As we saw there, this may not be enough. The shock in the height error almost certainly points to a residual lack of ‘smoothness’ in the boundary fields. More rigorous mathematical guidance is needed. The issue of the need for smoothness when the boundary conditions are slightly inaccurate but contain useful information, has not, to my knowledge, been addressed in the context of transparent boundary conditions. In another context Browning and Kreiss (1982) made the point that if the boundary conditions ‘are incorrect but smooth then we also showed that the ensuing solution was smooth. Unfortunately the error propagates at inertial/gravity wave speed so that the boundary data errors must be kept small’.

Because it is early days, some of the following remarks concerning the strengths and weaknesses of transparent boundary conditions are speculative. (a) Stability: in principle, we should be able to prove this for linear systems; see, for example, the appendix of Elvius and Sundström (1973). Lie (2001) derived stability for the mixed finite element discretization and Lie (2000) gives error estimates. It is not clear, however, that stability can be proven for the non-linear case. (b) Robustness has not been tested in a meteorological context. However, the sensitivity to the initial data we discovered in section 2 is worrying. (c) These schemes are difficult to implement. The historical record speaks for itself. (d) Computational cost: this should be reasonable provided only lower order equations are needed. (e) Mass loss: ‘semi-transparent b.c.’ gave suspiciously bad behaviour. (f) Over-specifying the boundary: we are now imposing the correct number of fields on the boundary, thus minimising the errors caused by faulty host model fields. (g) Geostrophic balance: we are no longer destroying quasi-geostrophic balance in a zone adjacent to the boundary. (h) Tuning parameters: there are none. If the scheme fails,

it does so unambiguously. If it works, we do not have to re-tune any parameters if we change the grid size or time step. (i) Mathematically, its pedigree is excellent. (j) Residual reflections: waves for which  $f/(\bar{c}k)$  is large, and also waves striking the boundary at acute angles will be strongly reflected. We argued in section 2 that  $f/(\bar{c}k)$  is small for most waves in a meteorological context. Also, consider a plane wave making an angle of  $10^\circ$  with the western boundary. After reflection it will later approach the northern boundary making an angle of  $80^\circ$ , guaranteeing almost zero reflection.

The well-posedness of Eqs. (3.1)-(3.3) in combination with many of the boundary conditions listed in section 3 has been discussed by various authors. Sundström and Elvius (1979) demonstrated the well-posedness of the ‘ $\Phi$  b.c.’ and the ‘characteristic b.c.’. Giles (1990) extended this analysis to some higher order transparent boundary conditions. Hagstrom (1999) discusses the well-posedness of all higher order transparent boundaries. In an excellent review he also shows how to derive well-posed transparent boundaries for the linearized Navier-Stokes equations, which may be a step on the path to our ultimate destination: the most accurate possible boundary treatment for the non-hydrostatic equations.

If the strategies tested in this paper prove inadequate, there are others on offer; see Tsynkov (1998). A particularly intriguing one which comes from electromagnetic theory, is known as the Perfectly Matched Layer technique; Berenger (1994). From a Meteorological perspective, it is interesting because it removes what we called *weakness (i)* of the relaxation scheme in our introduction. We would think of it as a well-posed relaxation scheme. For an application to the linearized Euler equations see Hu (2001).

Lastly, if we take the lesson from our experiments that it is essential for the imposed boundaries to be as balanced as possible, and apply it to nested multi-level models, then initializing the host model fields using the guest forecast model is probably advisable, particularly where the host model vertical levels, or orography, or physical parameterization schemes differ from those of the guest model. This may be expensive, but operationally it can be done off-line.

*Acknowledgement.* Thanks to Jim Hamilton for assistance with the graphics. Thanks to Per Uden and to an anonymous reviewer for their constructive criticism of the original manuscript.

## APPENDIX 1.

### List of variables and constants not defined in the text.

$a$	: Radius of the earth ( $6.371 \times 10^6$ m)
$\bar{c}$	: ( $= \sqrt{\bar{\Phi}}$ ) speed of adjustment wave ( $\text{m s}^{-1}$ )
$f$	: Coriolis parameter ( $\text{s}^{-1}$ )
$\bar{f}$	: averaged Coriolis parameter ( $\text{s}^{-1}$ )
$g$	: Acceleration due to gravity ( $9.80665 \text{ m s}^{-2}$ )
$h$	: Used as a superscript to designate the host fields.
$t$	: Time (s)
$u$	: Zonal velocity ( $\text{m s}^{-1}$ )
$\bar{u}$	: Constant Eastward advection velocity ( $\text{m s}^{-1}$ )
$v$	: Meridional velocity ( $\text{m s}^{-1}$ )
$\bar{v}$	: Constant meridional advection velocity ( $\text{m s}^{-1}$ )
$v_N$	: Outward pointing normal velocity ( $\text{m s}^{-1}$ )
$v_T$	: Tangential velocity ( $\text{m s}^{-1}$ )
$\lambda$	: Longitude
$\Omega$	: Angular speed of the earth ( $7.292 \times 10^{-5} \text{ s}^{-1}$ )
$\Phi$	: Geopotential ( $\text{g} \times \text{height}$ ) ( $\text{m}^2 \text{ s}^{-2}$ )
$\bar{\Phi}$	: Constant geopotential ( $9 \times 10^4 \text{ m}^2 \text{ s}^{-2}$ )
$\Phi_0$	: Constant geopotential ( $58012.8 \text{ m}^2 \text{ s}^{-2}$ )
$\theta$	: Latitude

## APPENDIX 2.

The derivation of the boundary conditions  $B_-$  listed in table 1 is described in this appendix.  $B_+$  can be derived in exactly the same way.

Multiplying Eq. (2.10) by  $(-\bar{c})$  and adding the result to Eq. (2.12) yields

$$\left[ \frac{\partial}{\partial t} + (\bar{u} - \bar{c}) \frac{\partial}{\partial x} \right] [\Phi - \bar{c}u] + \bar{c}\bar{f}v = 0. \quad (\text{A.1})$$

Substituting  $\bar{f}v$  from Eq. (A.1) into Eq. (2.24) we get the ‘upstream boundary condition’:

$$B_-^1 = \frac{1}{\bar{c}} \left[ \frac{\partial}{\partial t} + \bar{u} \frac{\partial}{\partial x} \right] [\Phi - \bar{c}u] \quad (\text{A.2})$$

Substituting  $\partial(\Phi - \bar{c}u)/\partial x$  from Eq. (A.1) into Eq. (2.24) we get the ‘pure boundary condition’:

$$B_-^1 = \frac{1}{\bar{c} - \bar{u}} \left[ \frac{\partial}{\partial t} [\Phi - \bar{c}u] + \bar{u}\bar{f}v \right] \quad (\text{A.3})$$

In Eq. (2.25) substitute  $\partial(\Phi - \bar{c}u)/\partial x - \bar{f}v$  from Eq. (A.1) and  $\bar{f}u$  from Eq. (2.11) and we get the following after re-arranging the terms:

$$B_-^2 = \frac{1}{2\bar{c}} \left[ \frac{\partial}{\partial t} + \bar{u} \frac{\partial}{\partial x} \right] \left[ 2 \frac{\partial}{\partial x} [\Phi - \bar{c}u] - \bar{f}v \right] \quad (\text{A.4})$$

Use Eq. (A.1) to substitute for  $\bar{f}v$  and re-arrange and we get the ‘upstream boundary condition’:

$$B_-^2 = \frac{1}{2\bar{c}^2} \left[ \frac{\partial}{\partial t} + \bar{u} \frac{\partial}{\partial x} \right] \left[ \frac{\partial}{\partial t} + (\bar{u} + \bar{c}) \frac{\partial}{\partial x} \right] [\Phi - \bar{c}u] \quad (\text{A.5})$$

Lastly, substitute  $\partial(\Phi - \bar{c}u)/\partial x$  from Eq. (A.1) in Eq. (2.25) and re-arrange:

$$B_-^2 = \frac{1}{\bar{c} - \bar{u}} \left[ \frac{\partial^2}{\partial t \partial x} [\Phi - \bar{c}u] + \bar{u} \bar{f} \frac{\partial v}{\partial x} \right] + \frac{\bar{f}^2}{2\bar{c}} u. \quad (\text{A.6})$$

Substitute  $\partial(\Phi - \bar{c}u)/\partial x$  from Eq. (A.1) and  $\bar{u}\partial v/\partial x$  from Eq. (2.11) and, after re-arranging we get the ‘pure boundary condition’:

$$B_-^2 = \frac{1}{(\bar{c} - \bar{u})^2} \left[ \frac{\partial^2}{\partial t^2} [\Phi - \bar{c}u] + \bar{u} \bar{f} \frac{\partial v}{\partial t} + \frac{\bar{u}^2 - \bar{c}^2}{2\bar{c}} \bar{f}^2 u \right] \quad (\text{A.7})$$

## 6. REFERENCES.

- Baumhefner D.P and D.J. Perkey 1982: Evaluation of lateral boundary errors in a limited-domain model. *Tellus*, **34**, 409-428.
- Berenger, J-P, 1994: A perfectly matched layer for the absorption of electromagnetic waves. *J. Comp Phys.*, **114**, 185-200.
- Bourgeault, P., 1983: A non-reflective upper boundary condition for limited-height hydrostatic models. *Mon. Wea. Rev.*, **111**, 420-429.
- Browning, G. and H-O Kreiss 1982: Initialization of the shallow water equations with open boundaries by the bounded derivative method. *Tellus*, **34**, 334-351.
- Cats, G.J., and O. Åkesson, 1983: An investigation into a marked difference between two successive ECMWF forecasts of September, 1982. *Beitr. Phys. Atmosph.*, **56**, 440-451.
- Charney, J.G., 1962: Integration of the primitive and balanced equations. *Proceedings of the international symposium on numerical weather prediction, Tokyo, Meteor. Soc. Japan*, 131-152.
- Charney, J.G., R. Fjørtoft and J. von Neumann, 1950: Numerical integration of the barotropic vorticity equation *Tellus*, **2**, 237-254.
- Davies, H.C., 1976: A lateral boundary formulation for multi-level prediction models. *Q. J. Roy. Met. Soc.*, **102**, 405-418.
- Davies, H.C., 1983: Limitations on some common lateral boundary schemes used in regional NWP models. *Mon. Wea. Rev.* **111**, 1002-1012.
- Durrant, D.R., M.-J. Yang, D.N. Slinn and R.G. Brown, 1993: Toward more accurate wave-permeable boundary conditions. *Mon. Wea. Rev.*, **121**, 604-620.
- Elvius, T., 1977: Experiments with a primitive equations model for limited area forecasts. *Beitr. Phys. Atmosph.*, **50**, 367-392.
- Elvius, T. and A. Sundström, 1973: Computationally efficient schemes and boundary conditions for a fine mesh barotropic model based on the shallow water equations. *Tellus*, **25**, 132-156.
- Engquist, B., and A. Majda, 1977: Absorbing boundary conditions for the numerical simulation of waves. *Math. Comput.*, **31**, 629-651.

- Giles, M., 1990: Non-reflecting boundary conditions for Euler equation calculations *AIAA Journal*, **28**, 2050-2058.
- Givoli, D., 1992: *Numerical methods for problems in infinite domains*. Amsterdam: Elsevier.
- Gustafsson, B., H.-O. Kreiss and A. Sundström, 1972: Stability theory of difference approximations for mixed initial boundary value problems. II. *Math. Comput.*, **26**, 649-686.
- Hagstrom, T., 1999: Radiation boundary conditions for the numerical simulation of waves. *Acta Numerica*, **8**, 47-106.
- Holstad, A., and I. Lie, 2001: Transparent boundary conditions using a mixed finite element formulation of the shallow water equations. *DNMI Research Report 120* 48pp. Available from Ivar Lie, DNMI, P.O.Box 43 Blindern, N-0313 Oslo, Norway.
- Hu, F.Q., 2001: A stable perfectly matched layer for linearized Euler equations in unsplit physical variables. *J. Comp Phys.*, **173**, 455-480.
- Klemp, J.B., and D. Durran, 1983: An upper boundary condition permitting internal gravity wave radiation in numerical mesoscale models. *Mon. Wea. Rev.*, **111**, 430-444.
- Källén, E., 1996: HIRLAM documentation manual. Available from Erland Källén, SMHI, S-60176 Norrköping, Sweden.
- Källberg, P., 1977: Test of a lateral boundary relaxation scheme in a barotropic model. *ECMWF research department internal report no. 3*, 21pp.
- Laprise, R., Varma, M.R., Denis, B., Caya, D. and I. Zawadzki, 2000: Predictability of a nested limited-area model. *Mon. Wea. Rev.*, **128**, 4149-4154.
- Lehmann, R., 1993: On the choice of relaxation coefficients for Davies' lateral boundary scheme for regional weather prediction models. *Meteor. Atmos. Phys.*, **52**, 1-14.
- Lie, I., 2000: Error estimates for the shallow water equations with transparent boundary conditions and semi-Lagrangian time discretization. *DNMI Research Report 111* 15pp. Available from Ivar Lie, DNMI, P.O.Box 43 Blindern, N-0313 Oslo, Norway.
- Lie, I., 2001: Well-posed transparent boundary conditions for the shallow water equations. *Appl. Numer. Math.*, **38**, 445-474.
- Lynch, P., 1996: The Dolph-Chebyshev window: a simple optimal filter. *Mon. Wea. Rev.*, **125**, 655-660.
- McDonald, A., 1997: Lateral boundary conditions for operational regional forecast models; a review. *HIRLAM technical report 32* Available from A. McDonald, Irish Meteorological Service, Glasnevin Hill, Dublin 9, Ireland.
- McDonald, A., 1998: Conservation of mass in HIRLAM. *HIRLAM newsletter 32*, 39-44. Available from A. McDonald, Irish Meteorological Service, Glasnevin Hill, Dublin 9, Ireland.
- McDonald, A., 1999: Well-posed boundary conditions for semi-Lagrangian schemes: the one-dimensional case. *HIRLAM technical report 43*. Available from A. McDonald, Irish Meteorological Service, Glasnevin Hill, Dublin 9, Ireland.
- McDonald, A., 2000: Well-posed boundary conditions for semi-Lagrangian schemes: the one-dimensional case. Part II. *HIRLAM technical report 44*. Available from A. McDonald, Irish Meteorological Service, Glasnevin Hill, Dublin 9, Ireland.
- McDonald, A., 2002: A step toward transparent boundary conditions for meteorological models. *Monthly Weather Review*, **130**, 140-151.

- McDonald, A., and J.E. Haugen, 1992: A two time level, three dimensional semi-Lagrangian and semi-implicit grid point model. *Monthly Weather Review*, **120**, 2603-2621.
- Mesinger, F., 1977: Forward-backward scheme and its use in a limited area model. *Beitr. Phys. Atmosph.*, **50**, 200-210.
- Norbury, J., and M.P.J. Cullen, 1985: A note on the properties of the primitive hydrostatic equations of motion. *Quart. J. Roy. Meteor. Soc.*, **111**, 1135-1137.
- Oliger, J. and A. Sundström, 1978: Theoretical and practical aspects of some initial boundary value problems in fluid dynamics. *S.I.A.M. J. Appl. Math.*, **35**, 419-446.
- Platzman, G.W., 1954: The computational stability of boundary conditions in numerical integration of the vorticity equation. *Arch. Met. Geoph. Biokl., Serie A*, **7**, 29-40.
- Sundström, A., 1969: Stability theorems for the barotropic vorticity equation. *Mon. Wea. Rev.*, **97**, 340-345.
- Sundström, A. and T. Elvius, 1979: Computational problems related to limited area modelling. *Numerical methods used in atmospheric models, vol. 2. (GARP publication series no. 17)*, 379-416.
- Tsynkov, S.V., 1998: Numerical solutions of problems on unbounded domains. A review. *Appl. Num. Math.* **27**, 465-532.
- Wagatha, L., 1983: Approximation of pseudodifferential operators in absorbing boundary conditions for hyperbolic equations. *Numerische Mathematik* **42** 51-64. ! end of noindent for references.

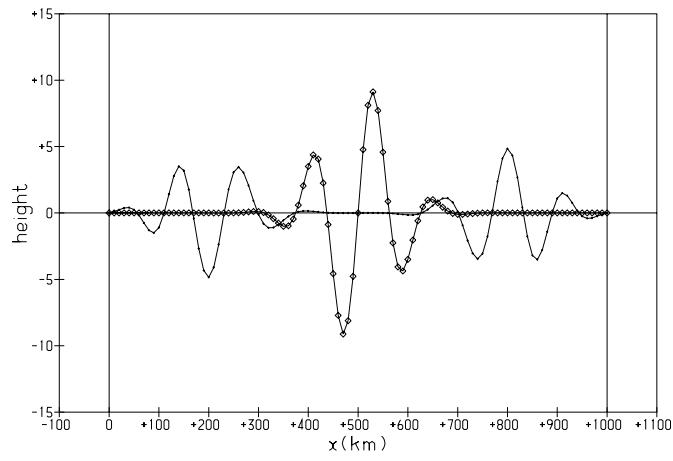


Figure 1: *The adjustment of an unbalanced wave packet: the diamonds display  $\Phi$  at time zero. The dots display the result of a 0.694444239hr integration, at which the leading edge of the two adjustment waves should have moved 750km.  $\Phi(0, t) = 0$  and  $\Phi(L, t) = 0$  have been imposed on the boundaries.*

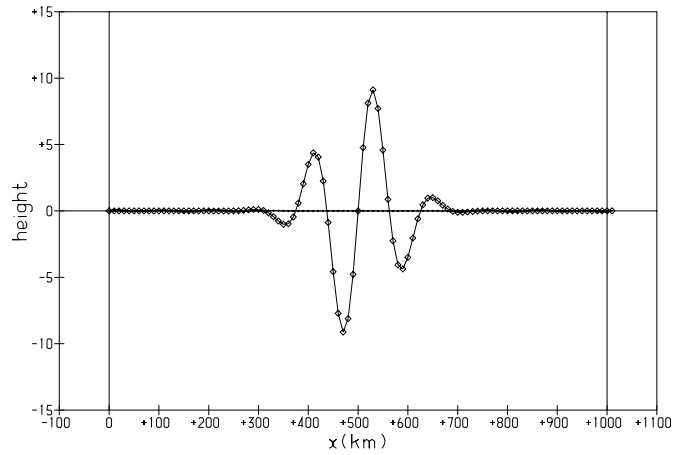


Figure 2: *Same as figure 1, but now imposing  $p(0, t) = 0$  and  $q(L, t) = 0$  on the boundaries.*

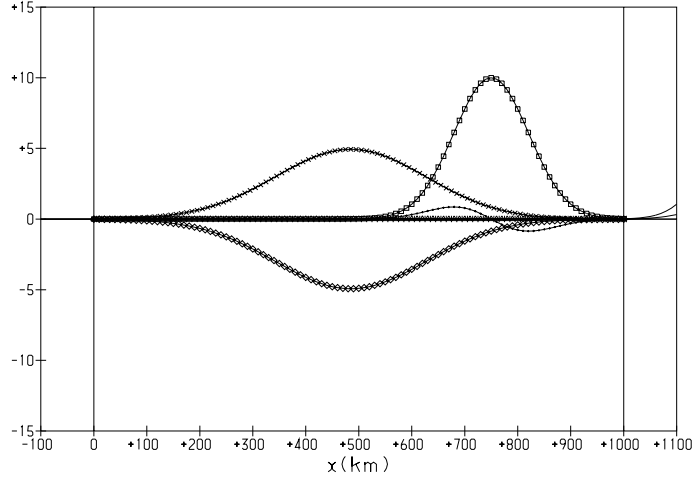


Figure 3: *The advection of a balanced bell shape out of the area imposing  $p(0, t) = 0$  and  $B_-^0(L, t) = \Phi(L, t) - \bar{c}_K u(L, t) = 0$  on the boundaries. At time zero, the squares display the height field, the plusses the  $c_K u$ -field, and the dots the  $v$ -field. At time  $T$  the diamonds display the height field, the exes the  $c_K u$ -field, and the triangles the  $v$ -field, which are difficult to see because  $v = 0$ .*

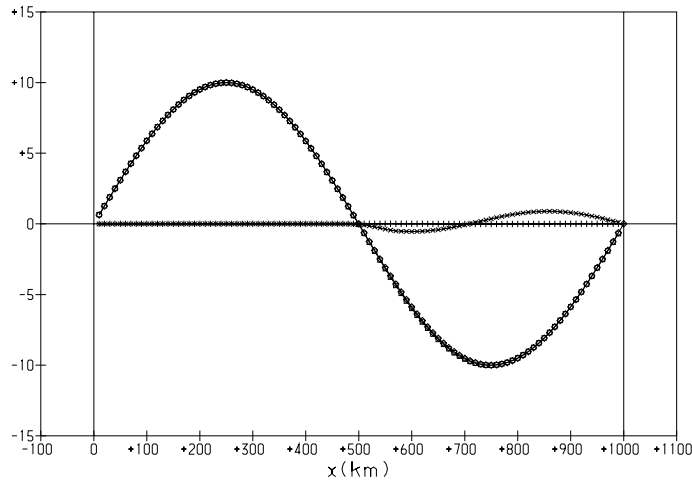


Figure 4: *Plot of  $(\Phi + \bar{\Phi}u/\bar{c}_K)/2$  and  $(\Phi - \bar{\Phi}u/\bar{c}_K)/2$ . The initial field is a pure  $\omega_+$ -wave whose wavelength is  $L$ ;  $(\Phi + \bar{\Phi}u/\bar{c}_K)/2$  is plotted as diamonds and  $(\Phi - \bar{\Phi}u/\bar{c}_K)/2$  is plotted as plusses. At time  $T$ ,  $(\Phi + \bar{\Phi}u/\bar{c}_K)/2$  is plotted as squares and  $(\Phi - \bar{\Phi}u/\bar{c}_K)/2$  is plotted as exes. At  $x = 0$ , we impose the analytical solution. At  $x = L$  we impose  $B_-^1(L, t) = 0$ .*

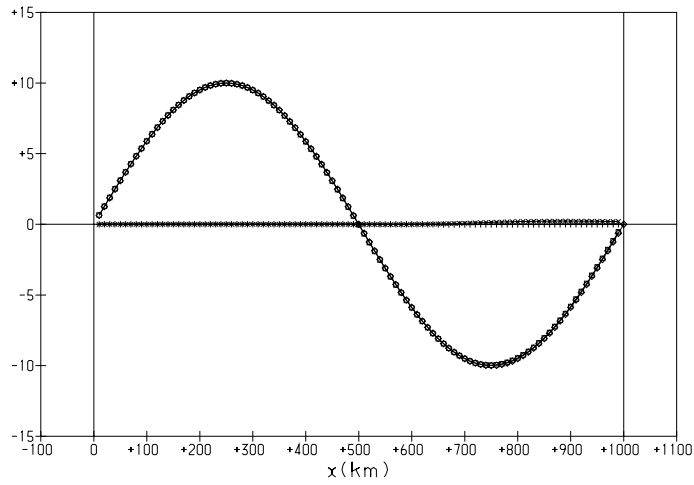


Figure 5: *Same as figure 4, except we now impose  $B_-^2(L, t) = 0$  at  $x = L$ .*

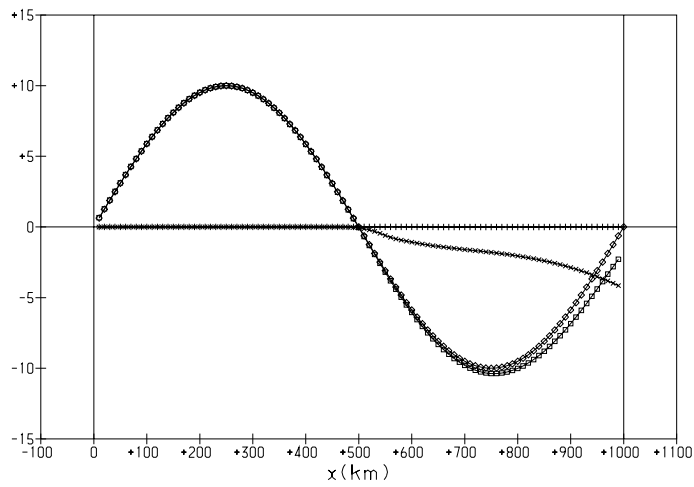


Figure 6: *Same as figure 5, except we now impose a single incorrect datum: an erroneous value of  $q(L, -\Delta t) = q(L, 0)$ , instead of the analytical value of  $q(L, -\Delta t)$ .*

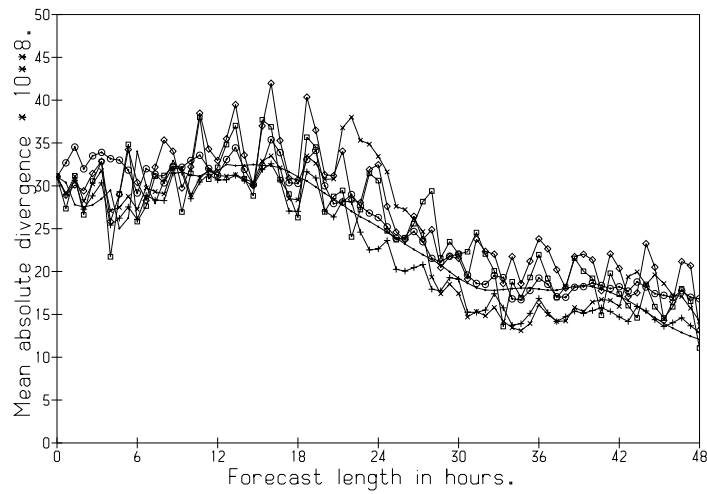


Figure 7: Graph of the evolution of  $\overline{|D|}$  multiplied by  $10^8$  computed over the guest area during the 48h guest model forecast. The key to the symbols is as follows. ‘S.L.b.c.’: diamonds, ‘ $\Phi$  b.c.’: squares, ‘characteristic b.c.’: plusses, ‘semi-transparent b.c.’: crosses, ‘relaxation b.c.’: circles, the host fine mesh values computed over the guest area: dots.

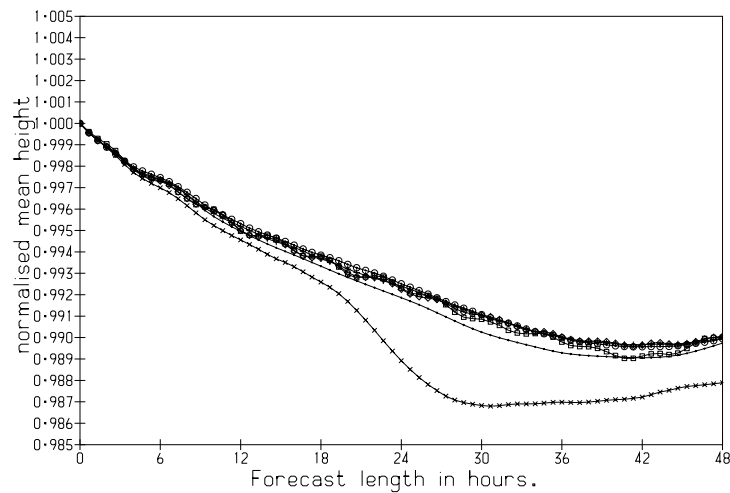


Figure 8: Graph of the evolution of the mean value of  $\Phi$  computed over the guest area during the 48h guest model forecast. It is normalized so that it equals 1 at time zero. The key to the symbols is the same as in figure 7.

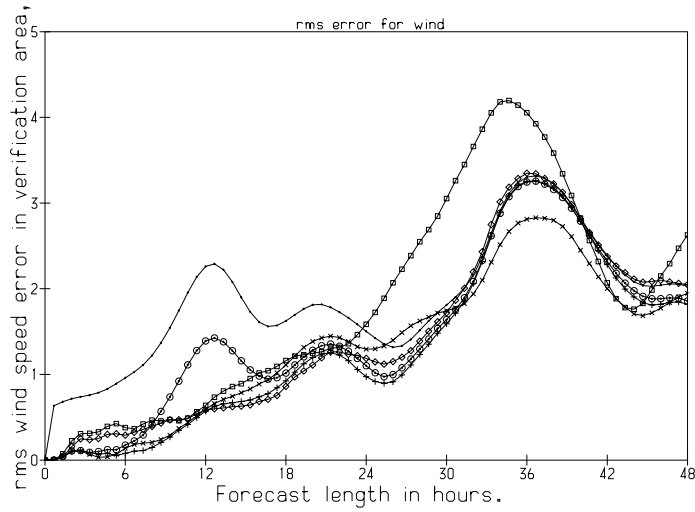


Figure 9: *Graph of the evolution of the rms wind errors computed over the verification area during the 48h guest model forecast. The key to the symbols, except the dots is the same as in figure 7. The dots show the rms wind errors for the coarse mesh host integration computed over the verification area.*

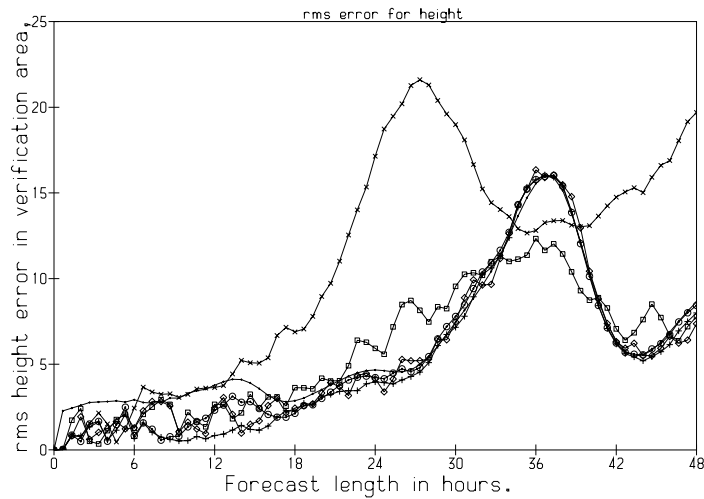


Figure 10: *Graph of the evolution of the rms height errors computed over the verification area during the 48h guest model forecast. The key to the symbols, except the dots is the same as in figure 7. The dots show the rms height errors for the coarse mesh host integration computed over the verification area.*